longer is able to excite an intense wakefield. The speed at which the ionization contour erodes backwards scales [19] as ionization potential (IP) to the power 1.73. This is because atoms of a gas that have a lower ionization potential will be ionized earlier during the rising charge density of the beam and thus the beam will propagate further before it completely "diffracts" away due to the beam emittance. Thus the 20.3 GeV electron beam is expected to propagate 40% further (and therefore give a correspondingly higher energy gain) in a self-ionized Rb (ionization potential IP 4.4 eV) plasma, compared to the previously used Li (IP 5.1 eV) plasma.

A second motivation for exploring Rb is the need to mitigate emittance dilution of the electron beam due to possible ion motion [5] in future applications. In the "blow-out" regime[16] referred to earlier, the plasma electrons are completely blown out, leaving behind a region that contains the more massive, less mobile ions. This ion column exerts a linear focusing force on the electron beam, which preserves the transverse phase space of a matched beam [7], i.e. with $\sigma_r^2 = \epsilon_n(c/\omega_p)\sqrt{2/\gamma}$. If the density of the beam is large enough— $(n_b/n_p) > m_i/m_e$— the ions are attracted toward the electron beam axis and the focusing force of the resulting ion column is no longer linear which will in turn lead to the growth of the normalized emittance ϵ_n [5]. Since the extent of the ion motion scales inversely with the mass of the ions, heavier Rb atoms are preferred over the previously used Li atoms.

The experiments were carried out at the FACET facility with the setup shown in Fig 1. The 20.3 GeV electron bunch, containing 1.8×10^{10} particles with $\sigma_z \sim 35 - 50\mu m$ [20] was focused to a vacuum σ_r of $35\mu m$ at the beginning of the plateau region (i.e. after the up-ramp, described below) of the Rb vapor in a heat pipe oven [21]. The electrons within the bunch were used to ionize Rb, excite a wake, and probe it [6].

The rubidium vapor was collisionally contained in the hot region of the oven by an argon buffer gas. The rubidium density profile can be approximated by a trapezoidal shape with 10 cm up-ramp, 20 cm plateau region, and 10 cm down-ramp. In the 10 cm long boundary region on either side of the heated region, the density of argon must rise as the rubidium density falls to maintain pressure balance. In the central 20 cm long heated region, the Rb density is nearly constant at $2.7 \times 10^{17} cm^{-3}$.

The total charge that enters and leaves the heat pipe oven is measured using two absolutely calibrated toroids. The downstream toroid measures the beam charge plus any accelerated excess charge(ΔQ) from further ionization of Rb and Ar. Second, the dispersed spectrum of the beam electrons is recorded by camera C, an example of which is shown in Fig 1(b). The spectra are first summed in the non-dispersed direction and then integrated along the dispersed direction. The running integral is shown as the white curve in Fig 1(b) which
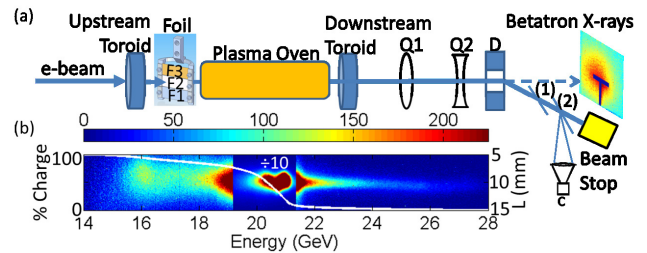

FIG. 1. (a)The experimental setup. The dipole (D) and quadrapole magnets(Q1 and Q2) form the imaging spectrometer used as the energy diagnostic, Cerenkov radiation produced in air between Si wafers (1) and (2) is recorded using a 12 bit camera (C). Foils can be inserted in the beam (arrow) as it enters the plasma to change ϵ_N by factors of 1.2 (F1), 1.3(F2), and 1.4(F3), respectively from the nominal value of $\epsilon_{N0} = 250 \times 50\mu m$ without any foils. The Lanex screen, placed behind a 1mm copper sheet, is the betatron x-ray diagnostic; (b)an example of the energy spectrum with the white curve showing the percentage of the total beam charge. The charge near 21 GeV, observed not to lose any energy, has been attenuated by factor 10 on the image. The electron bunch has a head-to-tail correlated energy spread of 0.5 GeV.

is used to define the maximum energy (2% of the total charge) and the minimum energy (98% of the total charge) of the electrons. We use these levels to calculate $\langle T \rangle \equiv \Delta W^+/\Delta W^- = \int E^+ dz/\int E^- dz$, taking into account the initial head-to-tail correlated energy spread of the electrons. Since the electron bunch is ultra-relativistic, there is no relative motion between the particles, so the change in energy of any longitudinal slice of the beam is equal to the axially integrated electric field at the location of that slice over the length of the interaction.

As the bunch enters the up-ramp region, the electric field of the rising edge of the bunch easily ionizes the Rb atoms to Rb^+ and begins to blow out the plasma electrons. The experiment rapidly evolves into the blow-out regime as the focusing force of the ions pinches the initially $\sigma_r = 35\mu m$ beam to $\sigma_r^* = 3\mu m$, after which its envelope oscillates along the entire length of the ion column [11]. These envelope oscillations have a calculated wavelength of about 0.9 cm based on the experimental parameters. If σ_r^* is small enough, the combined action of the beam's radial field E_r and the wakefield E_z can ionize Rb^+ to Rb^{2+}. The threshold electric field (defined here as 10% ionization level) needed to produce Rb^{2+} (IP= 27.3 eV) is calculated using the ADK theory [22] as 53 GV/m. Taking σ_r^* of 3 μm, we can estimate the maximum E_r at the peak of the bi-Gaussian beam to be $E_r^{\max} = 17.3 GV/m(N/10^{10})(10\mu m/\sigma_r^*)(30\mu m/\sigma_z) = 56$ GV/m. Thus, the electron bunch produces Rb II electrons along the length of the plasma at the minimum of each slice of the beam as it executes envelope oscillations. Since the bunch loses energy in the decelerating portion of the wake along this length, we expect there to be a
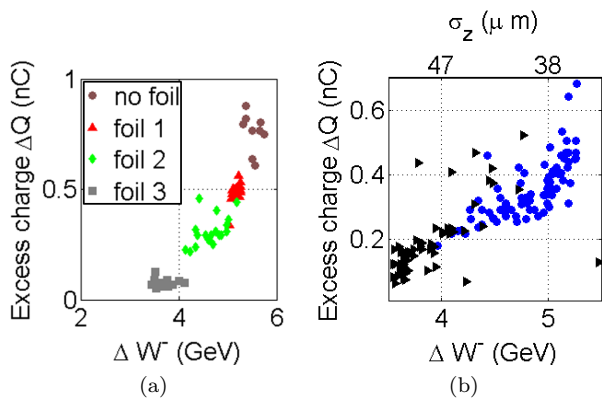
FIG. 2. (a)Excess charge ΔQ as a function of energy loss ΔW^- for 4 different beam propagation lengths in the plasma determined by changing ϵ_n by inserting foils in the path of the beam($\sigma_z = 40\mu m$); (b) ΔQ as a function of ΔW^- as the peak current of the beam is changed by changing σ_z. Estimated bunch length is given on the scale at the top [23] ($\epsilon_N = 1.3\,\epsilon_{N0}$, Foil 2). The variation in σ_z is either from shot to shot variation or from a change in bunch compression setting (shorter bunch setting as blue circles, longer bunch setting as black triangles). Linear fit to the observed correlation between ΔW^- and σ_z is used to obtain the σ_z scale in this figure.
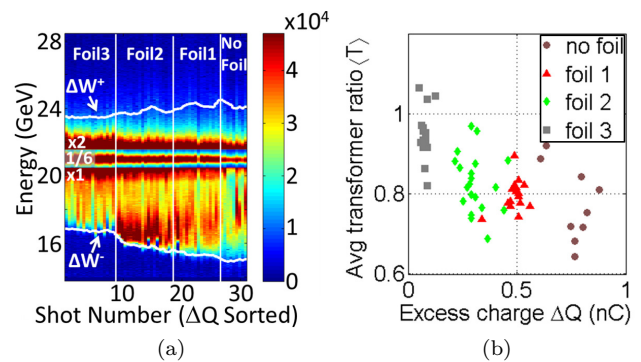

FIG. 3. (a) Measured energy spectra of the same shots as displayed in Fig 2(a). The values of energy loss ΔW^- and gain ΔW^+ are shown as white lines and are displayed as a moving average of 5 shots. The numbers on the left hand side indicate the factors used on the data in the three primary energy ranges for better visibility, (b) the measured average transformer ratio $\langle T \rangle = \Delta W^+ / \Delta W^-$ as a function of excess charge ΔQ leaving the plasma.

strong correlation between the energy loss and the excess charge in the experiment. Note that although the beam envelope oscillations could in principle be eliminated by matching the beam to the plasma, the envelope radius of the matched beam has to be large enough so that the combined field of the electron beam and the wake does not exceed the ionization threshold of the rubidium.

Distributed production of dark current is demonstrated from the correlation of ΔQ with the energy loss of the electron bunch, which increases as the bunch propagates further into the plasma. This distance, which can be less than the oven length, may be modified by varying either the beam emittance ϵ_N or the beam current. Both factors affect the head erosion rate, which is proportional to ϵ_N, and $I^{-3/2}$ [4], where I is the peak beam current $\propto 1/\sigma_z$. We first vary ϵ_N (by inserting foils F1, F2, and F3 in the beam path) while keeping σ_z and therefore the current profile of the beam constant. From Fig 2(a), one can see that as the beam ϵ_N is decreased, ΔW^- and the excess charge ΔQ increase. This is because a decrease in ϵ_N decreases the head erosion rate, thereby increasing the bunch propagation distance (and therefore ΔW^-) in the plasma. The increase in ΔQ occurs due to a combination of a decreased σ_r^* in the ion column and a longer propagation distance in the plasma.

Next, the beam propagation length is increased by increasing the beam current i.e. by reducing σ_z(while keeping the ϵ_N constant) to show that the increase in ΔQ is a result of a longer propagation length rather than a change in σ_r^*. As Fig 2(b) shows, we once again see that as the ΔW^- increases, so does ΔQ. In this case, ΔQ is not

affected by σ_r^*, since σ_r^* does not depend on σ_z. Now the principal source of increase in both ΔW^- and ΔQ is an increase of the interaction length and E_z, which occur as σ_z is decreased. The first factor will increase ΔQ by increasing the number of envelope oscillations, while the latter will do the same by increasing net electric field $\sqrt{E_r^2 + E_z^2}$ available for ionization of Rb^+.

The reduction of $\langle T \rangle$ with increasing ΔQ can be visually observed on Fig 3(a), which shows the energy spectra of electron bunches for the same data points that are depicted in Fig 2(a). These spectra are arranged in order of increasing ΔQ with the divide between different beam emittance settings indicated. It can be observed that as ΔQ is increased, the 2% charge (energy gain) contour shows a slower increase than does the 98% charge (energy loss) contour. This results in a decrease in $\langle T \rangle$ values, which are plotted in Fig 3(b) for these same data points. It is clear that $\langle T \rangle$ reduces from about 1 to 0.75 as the excess charge increases from 0.1 to 0.8 nC. The variation in $\langle T \rangle$ at a given value of ΔQ is probably due to subtle differences in the number of electrons in the tail of the electron bunch current profile, whereas the change in ΔQ at a given $\langle T \rangle$ is probably due to small changes to σ_r^* that affect E_r and thus the ionization rate of Rb^+. Nevertheless, the general trend observed is that $\langle T \rangle$ decreases as ΔQ increases. This suggests that these Rb II electrons are beam loading the accelerating field and draining energy from the wake.

To show that beam loading by the Rb II electrons is the cause of the reduction of the transformer ratio, we have carried out particle-in-cell simulations using the code OSIRIS [24] in 2D cylindrical coordinates. The simulation box has 480×400 square cells, each having a size of 0.05 k_p^{-1}. Both Rb and Ar are included in the simulation. The ionization of Rb and Ar is modelled using
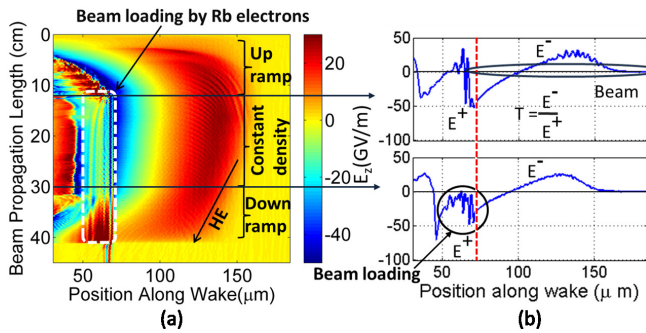
FIG. 4. 2D cylindrical OSIRIS Simulation of the experiment. (a) on axis electric field (E_z) as a function of the beam propagation distance in the plasma. The dashed white rectangle indicates where the wake gets severely beam loaded by ΔQ. The arrow marked HE shows the receding of the wake in the speed of light frame due to beam head erosion, (b) lineouts at two different locations (indicated by two horizontal arrows in (a)), the first one just at the end of the up-ramp, and the second one after 30 cm of propagation in plasma at the end of the flat density region. The location used to measure E^+ is shown in red dashed line and is the location of 2% beam charge at the end of the simulation. The effect of beam loading is evident in the bottom frame of (b) as a strong damping of the E^+ field (circle).

the ADK formalism [22]. We use 16 particles per cell for each simulated species, and electrons from the creation of Rb^+, Rb^{2+} and Ar^+ are tracked separately. The initial electron beam parameters and the plasma density profile are similar to those in the experiment.

We tracked the radius of one longitudinal slice of the beam (where the wakefield changes its sign and therefore electrons lose no energy-and indeed found that the RbII electrons at this location were produced each time this slice pinched to its smallest size σ_r^*, adding to the ΔQ in a discreet and distributed fashion. In Fig 4(a), we show the variation of the on-axis E_z as a function of distance. One can clearly see the wavelength of the wake decreasing/increasing in the up/down ramp regions from 0-10cm and 30-40 cm, respectively. Also seen is the effect of near synchronous acceleration of excess charge (mostly Rb II electrons that overwhelm some Ar electrons injected in the up-ramp) on E_z from 10 cm onwards once the electron bunch enters the uniform Rb density region (the boxed region). Fig 4(b) shows two lineouts, one at 12 cm, where the beam loading is not yet severe , and the other at 30 cm, where the wake generated by the excess Rb II charge has nearly cancelled out the beam induced wake. This figure also shows that the value of T decreases from its weakly unloaded value of 1.4 ($E^+= 43$ GV/m) at a distance of 12 cm to about 1(E^+=26 GV/m) at 30 cm where the flat Rb density region ends. The $\langle T \rangle$ seen by the beam electrons is ~ 1, which takes into account the effect of the ramps. In the experiment, $\langle T \rangle$ values as low as 0.8 are observed which may be due to somewhat heavier beam loading of the first bucket by the excess charge.

We note that although nearly 0.8 nC of excess charge is produced in this experiment (mostly attributed to Rb II electrons), not all these electrons are necessarily being accelerated in the first bucket of the wake and thus do not contribute to beam loading. In the simulations, we observe that even though total ΔQ is up to 1 nC, only about 300 pC of Rb II electrons are injected and accelerated in the first bucket and contribute to the beam loading and reduction of T. This latter amount is consistent with the estimate based on conservation of energy arguments given at the beginning of this Letter.

In conclusion, we have shown through experiments and simulation that distributed injection of electrons due to beam-induced ionization of Rb^+ can beam load the wake and reduce the accelerating field and the transformer ratio.

[1] M. J. Hogan et al., New Journal of Physics **12**, 055030 (2010).
[2] P. Chen et al., Phys. Rev. Lett. **54**, 693 (1985).
[3] I. Blumenfeld et al., Nature **445**, 741 (2007).
[4] I. Blumenfeld, *Scaling of the longitudinal electric fields and transformer ratio in a non-linear plasma wakefield accelerator*, Ph.D. thesis, Stanford University (2009).
[5] J. Rosenzweig et al., Phys. Rev. Lett. **95**, 195002 (2005).
[6] M. J. Hogan et al., Phys. Rev. Lett. **95**, 054802 (2005).
[7] P. Muggli et al., Phys. Rev. Lett. **93**, 014802 (2004).
[8] C. Joshi et al., Phys. Plasmas **9**, 1845 (2002).
[9] R. Gholizadeh et al., Phys. Rev. Lett. **104**, 155001 (2010).
[10] T. Katsouleas et al., Part. Accel. **22**, 81 (1987).
[11] E. Oz et al., Phys. Rev. Lett. **98**, 084801 (2007).
[12] A. Pak et al., Phys. Rev. Lett. **104**, 025003 (2010).
[13] T. P. Rowlands-Rees et al., Phys. Rev. Lett. **100**, 105005 (2008).
[14] C. McGuffey et al., Phys. Rev. Lett. **104**, 025004 (2010).
[15] C. Clayton et al., Phys. Rev. Lett. **88**, 154801 (2002).
[16] W. Lu et al., Phys. Rev. Lett. **96**, 165002 (2006); J. Rosenzweig et al., Phys. Rev. A **44**, R6189 (1991).
[17] M. Tzoufras et al., Phys. Rev. Lett. **101**, 145002 (2008).
[18] D. Johnson et al., Phys. Rev. Lett. **97**, 175003 (2006).
[19] I. Blumenfeld et al., Phys. Rev. ST Accel. Beams **13**, 111301 (2010).
[20] A. Fisher and Z. Wu, private communication.
[21] P. Muggli et al., IEEE T. Plasma. Sci. **27**, 791 (1999).
[22] D. L. Bruhwiler et al., Phys. Plasmas **10**, 2022 (2003).
[23] Z. Wu et al., Rev. Sci. Instrum **84**, 022701 (2013).
[24] R. A. Fonseca et al., in *Lecture Notes in Computer Science*, Vol. 2331 (Springer Berlin Heidelberg, 2002) pp. 342–351.